

3-D MODELING AND AUTOMATIC REGRIDDING
IN SHAPE DESIGN SENSITIVITY ANALYSIS*

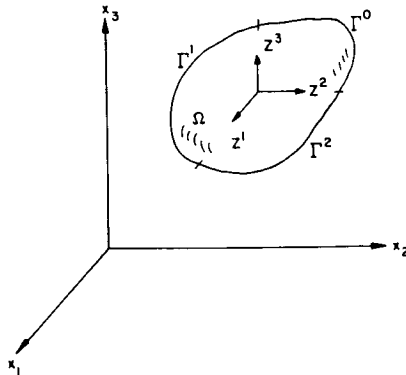
Kyung K. Choi and Tse-Min Yao
The University of Iowa
Iowa City, Iowa

The material derivative idea of continuum mechanics (Ref. 1) and the adjoint variable method of design sensitivity analysis are used to obtain a computable expression for the effect of shape variations on measures of structural performance of three-dimensional elastic solids (Ref. 2).

Consider the three-dimensional elastic solid shown in Figure 1, with the shape of the domain Ω as a design variable. In Figure 1, $z = [z^1, z^2, z^3]^T$ is the displacement field and Γ^0, Γ^1 , and Γ^2 are clamped, traction free, and loaded boundaries, respectively.

Using the principle of virtual work, the variational equilibrium equation for the elastic solid can be obtained (Ref. 3), where $\sigma^{ij}(z)$ and $\epsilon^{ij}(\bar{z})$ are the stress tensor due to a displacement z and the strain tensor due to a kinematically admissible virtual displacement \bar{z} , respectively, $f = [f^1, f^2, f^3]^T$ is the body force, $T = [T^1, T^2, T^3]^T$ is the traction force, and Z is the space of kinematically admissible virtual displacement. When the Galerkin method is applied to the variational equilibrium equation for approximate solution, an approximate finite-element equation is obtained.

THREE DIMENSIONAL ELASTIC SOLID



- Principle of Virtual Work:

$$a_{\Omega}(z, \bar{z}) = \iiint_{\Omega} \left[\sum_{i,j=1}^3 \sigma^{ij}(z) \epsilon^{ij}(\bar{z}) \right] d\Omega$$

$$= \iiint_{\Omega} \left[\sum_{i=1}^3 f^i \bar{z}^i \right] d\Omega + \iint_{\Gamma^2} \left[\sum_{i=1}^3 T^i \bar{z}^i \right] d\Gamma = l_{\Omega}(\bar{z}),$$

for all $\bar{z} \in Z$

- FEM Equation is an approximate equation of the variational equation.

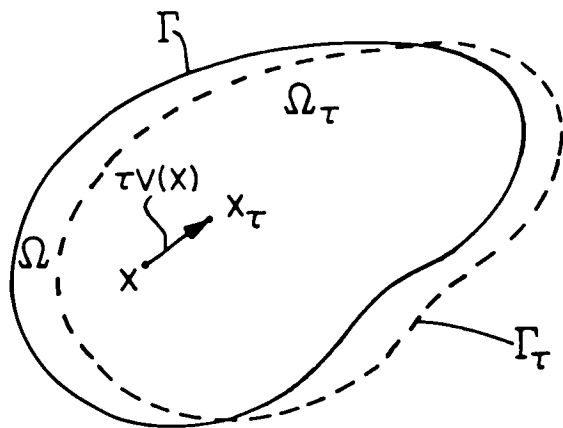
Figure 1

*Research supported by NASA Langley Grant NAG-1-215

Since the shape of domain Ω of the elastic solid is treated as the design variable, it is convenient to think of Ω as a continuous medium and utilize the material derivative idea of continuum mechanics. The process of deforming Ω to Ω_τ by mapping $\Omega_\tau = T(\Omega, \tau)$ may be viewed as a dynamic process of deforming a continuum, with τ playing the role of time. A design velocity field can be considered as a perturbation of design variable (Refs. 2 and 4).

Suppose $z_\tau(x_\tau)$ is a solution of the variational equilibrium equation on the deformed domain Ω_τ . Then the mapping $z_\tau(x_\tau) \equiv z_\tau(x + \tau v(x))$ is defined on Ω and $z_\tau(x_\tau)$ depends on τ in two ways. First, it is the solution of the boundary-value problem on Ω_τ . Second, it is evaluated at a point x_τ that moves with τ . Existence of the pointwise material derivative \dot{z} is shown in Ref. 2. If z_τ has a regular extension to a neighborhood U_τ of the closure $\bar{\Omega}_\tau$ of Ω_τ , then the partial derivative z' exists. One attractive feature of the partial derivative is that, with smoothness assumptions, it commutes with the derivative with respect to x_i (Ref. 2). (Fig. 2.)

VARIATION OF DOMAIN



$$x_\tau = T(x, \tau) = x + \tau V(x)$$

$$\Omega_\tau = T(\Omega, \tau)$$

$$V(x_\tau) \equiv \frac{dx_\tau}{d\tau} = \frac{\partial T(x, \tau)}{\partial \tau}$$

$$\begin{aligned} \dot{z} &= \left. \frac{d}{d\tau} z_\tau(x + \tau V(x)) \right|_{\tau=0} = \lim_{\tau \rightarrow 0} \frac{z_\tau(x + \tau V(x)) - z(x)}{\tau} \\ &= z'(x) + \nabla z^T V(x) \end{aligned}$$

$$\left(\frac{\partial z}{\partial x_i} \right)' = \frac{\partial}{\partial x_i} (z'), \quad i = 1, 2, 3$$

Figure 2

A common form of structural performance measure involves stress in an elastic solid. Consider a locally averaged stress functional ψ_p over a small subdomain $\Omega \subset \Omega$ of the elastic solid, as shown in Figure 3, where $g(\sigma)$ is a stress measure such as von Mises stress or principal stress and m_p is a characteristic function that has a constant value on Ω and its integral is 1. The averaged stress measure depends on shape of the domain in two ways; first directly on the domain over which the integral is carried out and second on the stress σ that, in turn, depends on the displacement field z .

Taking the first variation of ψ_p , using material derivative formulas of Refs. 2 and 5, ψ'_p is obtained. To obtain an explicit expression for ψ'_p in terms of the velocity field V , a variational adjoint equation is introduced by replacing $z \in Z$ by a virtual displacement $\bar{\lambda} \in Z$ and equating terms involving $\bar{\lambda}$ to the energy bilinear form $a_\Omega(\lambda, \bar{\lambda})$, yielding the variational adjoint equation for the adjoint variable λ .

STRESS SHAPE SENSITIVITY

$$\psi_p = \iiint_{\Omega} g(\sigma(z)) m_p \, d\Omega = \frac{\iiint_{\Omega} g(\sigma(z)) \, d\Omega}{\iint_{\Omega} d\Omega}$$

$$\psi'_p = \iiint_{\Omega} \left[\sum_{i,j=1}^3 g_{ij}(z) \sigma^{ij}(\dot{z}) \right] m_p \, d\Omega$$

$$- \iiint_{\Omega} \sum_{i,j=1}^3 \left[\sum_{k,\ell=1}^3 g_{ij}(z) c^{ijkl} (\nabla z^k v_\ell) \right] m_p \, d\Omega$$

$$+ \iiint_{\Omega} g \operatorname{div} V m_p \, d\Omega - \iiint_{\Omega} g m_p \, d\Omega \iiint_{\Omega} m_p \operatorname{div} V \, d\Omega$$

$$a_\Omega(\lambda, \bar{\lambda}) = \iint_{\Omega} \left[\sum_{i,j=1}^3 g_{ij}(z) \sigma^{ij}(\bar{\lambda}) \right] m_p \, d\Omega, \quad \text{for all } \bar{\lambda} \in Z$$

Figure 3

Using the adjoint variable method of design sensitivity analysis (Refs. 2 and 4) and the domain method of Ref. 5, an explicit and computable expression for ψ'_p in terms of the velocity field V is obtained. Evaluation of the design sensitivity ψ'_p requires the solution z of the original variational equation and the adjoint variable λ of the variational adjoint equation. This is an efficient calculation, using finite-element analysis, if the original variational equation for z has already been solved, requiring only evaluation of the solution of the same set of finite-element equations with a different right side, called an adjoint load.

For problems with smooth data in which stress is continuous, design sensitivity analysis results can be used for a pointwise stress functional. To obtain the formula, shrink the subdomain Ω_p to a point \hat{x} , where $\hat{x} \in \Omega$. In this case, the characteristic function becomes δ_p the Dirac delta measure.^p

Even though sensitivity analysis results for only a stress functional are presented here, the method is also applicable for displacement at a specified point \hat{x} and eigenvalue design sensitivity analysis, as shown in Refs. 2 and 5. (Fig. 4.)

$$\begin{aligned} \psi'_p &= \ell'_V(\lambda) - a'_V(z, \lambda) \\ &- \iiint_{\Omega} \sum_{i,j=1}^3 \left[\sum_{k,l=1}^3 g_{ij} \sigma_{ij}(z) c^{ijkl} (\nabla z^k v_l^T) \right] m_p d\Omega \\ &+ \iiint_{\Omega} g \operatorname{div} v_m d\Omega - \iiint_{\Omega} g m_p d\Omega \iiint_{\Omega} m_p \operatorname{div} v d\Omega \\ a'_V(z, \lambda) &= - \iiint_{\Omega} \sum_{i,j=1}^3 [\sigma^{ij}(z) (\nabla \lambda^i v_j^T) + \sigma^{ij}(\lambda) (\nabla z^i v_j^T)] d\Omega \\ &+ \iiint_{\Omega} \left[\sum_{i,j=1}^3 \sigma^{ij}(z) \epsilon^{ij}(\lambda) \right] \operatorname{div} v d\Omega \\ \ell'_V(\lambda) &= \iiint_{\Omega} \sum_{i=1}^3 \lambda^i (\nabla f^i v) d\Omega + \iiint_{\Omega} \left[\sum_{i=1}^3 f^i \lambda^i \right] \operatorname{div} v d\Omega \\ &+ \iint_{\Gamma^2} \left\{ - \sum_{i=1}^3 T^i (\nabla \lambda^i v) + (\nabla \left[\sum_{i=1}^3 T^i \lambda^i \right])^T n + H \left[\sum_{i=1}^3 T^i \lambda^i \right] (v^T n) \right\} d\Gamma \end{aligned}$$

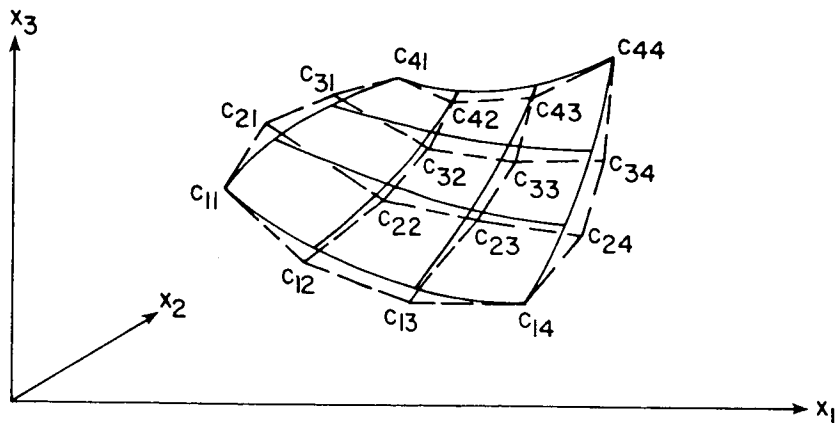
- Pointwise stress functional can be treated for problems with smooth data.

Figure 4

For numerical implementation of shape design sensitivity analysis, the boundary Γ of the domain Ω must be parameterized. There are several methods to parameterize the boundary Γ (Ref. 6). Since the result of shape optimization depends on the parameterization method used, it must be general and flexible enough to represent a large class of structural shapes. It is desirable that the parameterization method has the following properties: smoothness, fairness, required order of continuity, controllability in global and local senses, and a variation diminishing property. Among several parameterization methods, Bezier and B-spline surfaces are commonly used (Ref. 6). Both Bezier and B-spline surfaces use a set of blending functions and are defined in terms of characteristic polyhedra.

Points $p_{x_i}(v,w)$, $i = 1,2,3$, on a Bezier surface are constructed by taking linear combinations of a set of blending functions $B_{m,M}(v)$ and $D_{n,N}(w)$ and x_i coordinates c_{mnx_i} of control points (vertices of the characteristic polyhedron). A Bezier surface represented by a 4×4 array of points is shown in Figure 5. If a Bezier surface is used, positions c_{mnx_i} of the control points are shape design parameters.

MODELING FOR SHAPE (BEZIER SURFACE)



$$p_{x_i}(v,w) = \sum_{m=0}^M \sum_{n=0}^N c_{mnx_i} B_{m,M}(v) D_{n,N}(w), \quad i = 1,2,3$$

- Positions c_{mnx_i} of the control points are shape design parameters.

Figure 5

The next step is to develop a general method of defining and computing a velocity field in the domain, in terms of the perturbations of the positions of control points. It is shown in Ref. 7 that regularity of the velocity field must be at least at the level of regularity of the displacement field of the structure. This suggests use of displacement shape functions to systematically define the velocity field in the domain. Moreover, a velocity field that obeys the governing (elliptic) equation of the structure can be selected. That is, a perturbation of the boundary can be considered as a displacement at the boundary. With no additional external forces and a given displacement at the boundary, the finite-element equation can be used to find the displacement (domain velocity) field, where $\{V_b\}$ is the given perturbation of nodes on the boundary, $\{V_d\}$ is the node velocity vector in the interior of the domain, and $\{f_b\}$ is the fictitious boundary force acting on the varying boundary.

To use ψ' in Figure 4 for sensitivity computation, first perturb design parameter b_i (positions of control points), $i=1, 2, \dots, k$, a unit magnitude to obtain a boundary perturbation $\{V_b\}$. Then domain velocity $\{V_d\}$ is obtained. Using $\{V_d\}$ and displacement shape functions, ψ' in Figure 4 can be evaluated, which gives $\partial\psi/\partial b_i$. This method requires k solutions of the velocity equation. However, much as in adjoint analysis, this is an efficient calculation, requiring only evaluation of the solution of the same set of finite-element equations with a different right side for each unit perturbation of b_i , $i=1, 2, \dots, k$. (Fig. 6.)

AUTOMATIC REGRIDDING FOR SHAPE DESIGN

- Regularity of the velocity field must be the same as that of the displacement field
- Use of displacement shape functions to define velocity field
- Velocity field gives transformation mapping $T(x, \tau)$

$$\begin{bmatrix} K_{bb} & K_{bd}^T \\ K_{bd} & K_{dd} \end{bmatrix} \begin{Bmatrix} v_b \\ v_d \end{Bmatrix} = \begin{Bmatrix} f_b \\ 0 \end{Bmatrix}$$

$$[K_{dd}] \{v_d\} = - [K_{bd}] \{v_b\}$$

- Solve above equation k -times
- Excellent for boundary layer and/or substructuring technique

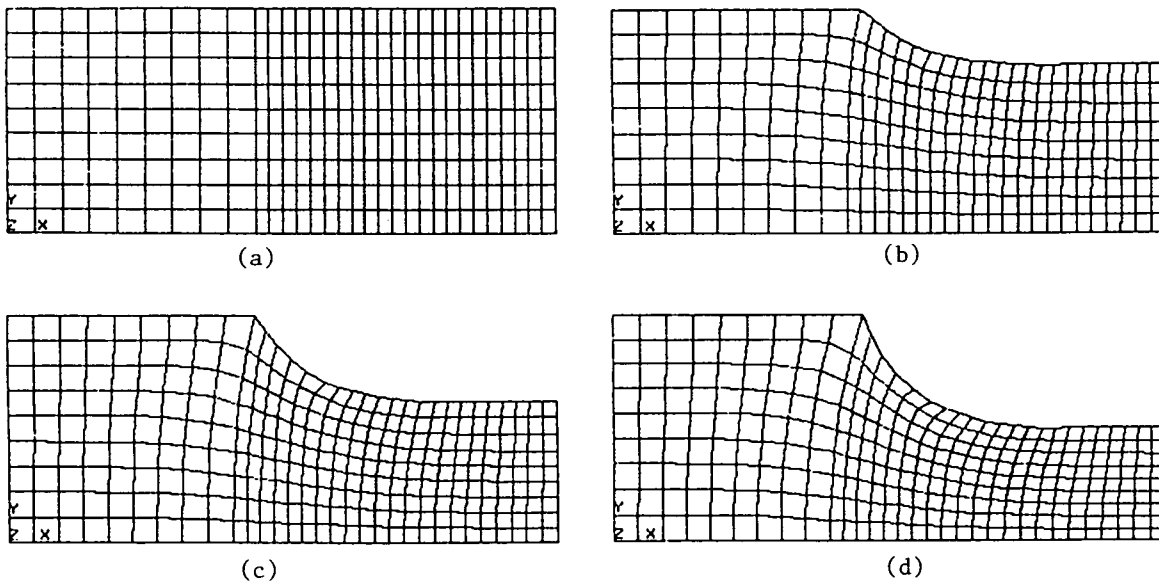
Figure 6

The automatic regridding method presented in Figure 6 can be used with the boundary-layer approach (Ref. 8) and/or substructuring techniques very effectively. That is, if a large portion of the structure is fixed, except for the boundary layer (or substructure), then the part of $\{V_d\}$ that corresponds to the fixed portion can be set equal to zero, thus reducing the dimension of $[K_{dd}]$.

Once a design change has been determined using an iterative design process, regridding of interior grid points can be carried out using $\{V_d\}$. If the initial grid is optimized using an adaptive method (Ref. 9), the regridding method presented will tend to avoid distortion of the finite elements.

To illustrate use of the automatic regridding method, a fillet problem (Figure 7) is used. In Figure 7, regridding is performed at three stages. It is interesting to observe that the method has a tendency to maintain orthogonality of the elements. That is, if the initial grid is regular, then the deformed grid tends to be regular. Also, the method presented can be utilized as mesh generator. That is, starting from a regular shape with a regularly patterned mesh (Figure 7(a)), the present method can be used to generate a mesh (Figure 7(d)) directly (Ref. 10).

AUTOMATIC REGRIDDING FOR FILLET PROBLEM



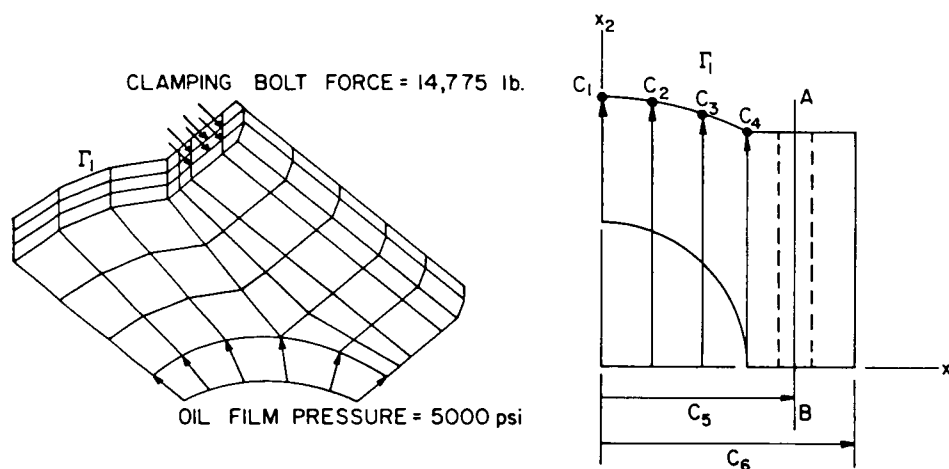
- The method can also be used as a mesh generator.

Figure 7

To demonstrate use of the automatic regriding method for shape design, an engine bearing cap (Ref. 11), subject to oil film pressure and a bolt load, is treated (Figure 8). Oil film pressure is a radial pressure loading, assumed to be uniform. The engine bearing cap is modeled as a three dimensional elastic solid. Due to symmetry, only the right half of the cap is analyzed. The finite-element configuration and loading conditions are shown in Figure 8. The material used is steel, with Young's modulus and Poisson's ratio of $E = 1.0 \times 10^7$ psi and $\nu = 0.3$, respectively. The finite-element model shown in Figure 8 contains 82 elements, 768 nodal points, and 2111 active degrees of freedom. For analysis and design velocity fields, the ANSYS finite-element STIF 95 (Ref. 12), which is a 20-node isoparametric element, is used. As in Ref. 13, implementation of design sensitivity analysis is performed outside the ANSYS finite element code.

The shape design variables for this problem are: The shape of the varying surface Γ_1 , distance c_5 of clamping bolt center line AB, and distance c_6 of edge from the cap centerline. For surface Γ_1 , a Bezier surface with a 4×4 array of points is used. For simplicity, only x_2 -coordinates of four control points c_1 through c_4 are allowed to vary. That is, surface Γ_1 has curvature in the x_1 -direction only.

ENGINE BEARING CAP



- ANSYS STIF95 (20-Node Isoparametric element)
- 82 elements, 768 nodes, and 2111 active DOF

Figure 8

The expression for design sensitivity ψ'_p of averaged von Mises stress over individual finite elements is given in Figure 4, where $g(\sigma)$ is von Mises stress. Define ψ_p^1 and ψ_p^2 as the functional values for the initial design b and modified design $b + \delta b$, respectively. Let $\Delta\psi_p = \psi_p^2 - \psi_p^1$ and let ψ'_p be the predicted difference from sensitivity analysis. The ratio $\psi'_p/\Delta\psi_p$ times 100 is used as a measure of accuracy; i.e., 100% means that the predicted change is exactly the same as the actual change. Notice this accuracy measure will not give meaningful information when $\Delta\psi_p$ is very small compared to ψ_p^1 , because the difference $\Delta\psi_p$ may lose precision due to the subtraction $\psi_p^2 - \psi_p^1$.

Numerical result with a 1% uniform design change; i.e., $\delta b = 0.01 b$, are shown in Figure 9 for randomly selected finite elements. Results given in Figure 9 show excellent agreement between predictions ψ'_p and actual changes $\Delta\psi_p$, except in elements 5 and 57. However, the magnitudes of actual change $\Delta\psi_p$ are small for those elements.

**SHAPE DESIGN SENSITIVITY FOR ENGINE BEARING CAP, $\delta b = 0.01b$
(AVERAGED VON MISES STRESS OVER FINITE ELEMENTS)**

El. No.	ψ_p^1	ψ_p^2	$\Delta\psi_p$	ψ'_p	$(\psi'_p/\Delta\psi_p \times 100)\%$
1	9829.4564	9727.3229	- 102.1335	- 109.7298	107.4
5	11444.4800	11448.0190	3.5390	0.4482	12.7
10	17933.5910	17964.5170	30.9260	29.8750	96.6
14	34270.5140	34294.7650	24.2510	23.7614	98.0
20	12670.2480	12634.3500	- 35.8980	- 38.4216	107.0
26	7311.4083	6999.4094	- 311.9989	- 321.7022	103.1
30	7234.2502	7081.2085	- 153.0417	- 159.7947	104.4
35	13328.4650	13264.9790	- 63.4860	- 59.4243	93.6
39	44231.0680	42109.0220	-2122.0460	-2222.5504	104.7
44	5998.6512	5844.9335	- 153.7177	- 165.1199	107.4
48	6822.9614	6736.9477	- 86.0137	- 90.5011	105.2
53	13634.1000	12964.2560	- 669.8440	- 701.6882	104.8
57	6121.4120	6114.6667	- 6.7453	- 8.1242	120.4
62	7041.7283	6971.4204	- 70.3079	- 79.6051	113.2
66	4787.5653	4761.5085	- 26.0568	- 27.6278	106.0
71	6541.8233	6585.9308	44.1075	45.1422	102.4
75	3820.6962	3843.9362	23.2400	22.5210	96.9
80	6240.3854	6285.3485	44.9631	46.3209	103.0

Unit: psi

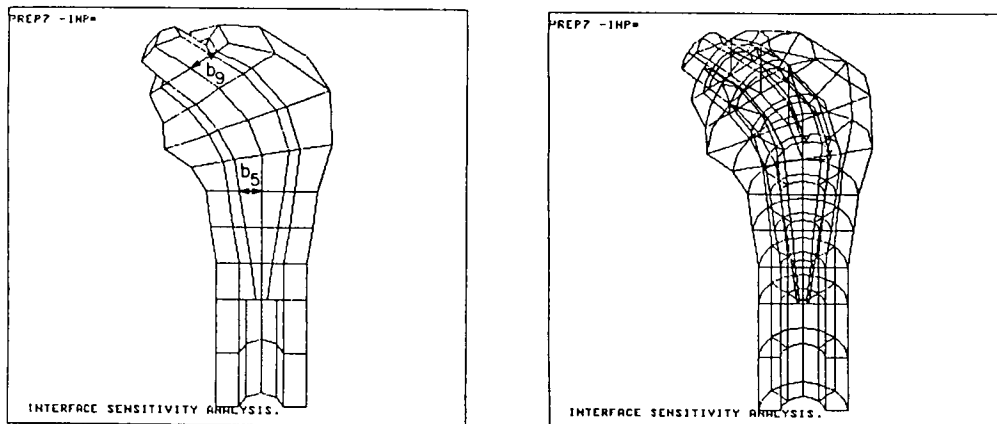
Figure 9

A total hip reconstruction consists of a three-dimensional elastic solid composed of cement, a metal stem, and cortical and trabecular bone (Figure 10). For simplicity, cortical and trabecular bone are modeled with the same material properties. Young's moduli and Poisson's ratios for metal stem, cement, and bone are: $E^1 = 207 \text{ GPa}$, $\nu^1 = 0.3$, $E^2 = 2.07 \text{ GPa}$, $\nu^2 = 0.23$, and $E^3 = 14.0 \text{ GPa}$, $\nu^3 = 0.3$, respectively.

The femur model shown in Figure 10 is obtained by approximating the real cadaver femur model of Ref. 14 with piecewise linear conical solids. For simplicity, structural and loading symmetries are assumed. Therefore, only half of the model is analyzed. A vertical load of 4000 N is applied at the tip of the metal stem.

The finite-element model consists of 16 elements for the metal stem, 28 elements for the cement, and 36 elements for the bone. ANSYS element STIF 95 is used for all finite elements. The model has 525 nodes and 1335 active degrees of freedom. The model is assumed to be fixed at the distal end of the bone.

TOTAL HIP RECONSTRUCTION (IMPLANT DESIGN)



- Pointwise stress and strain energy density at interface.
- 16 elements for stem, 28 elements for cement, and 36 elements for bone (all ANSYS STIF95).
- 525 nodes and 1335 active DOF.

Figure 10

There are 16 shape design parameters: b_1 through b_8 are the radius of the metal stem and b_9 through b_{16} are the radius of the outer surface of the cement, at different locations along the center line. Thus, $b_{i+8} - b_i$, $i=1,2,\dots,8$ is the thickness of the cement at those locations. The shape of the outer surface of the bone does not change.

The principal stress is used as a design failure criteria for the metal stem and bone, whereas strain energy density is considered as the design failure criteria for cement.

Shape design sensitivity results for pointwise principal stress in the stem at the stem-cement interface are given in Figure 11, for a 5% design change in design parameter b_5 . The pointwise stress is measured at a Gauss point (out of 9 Gauss points) on stem-cement interface of each stem finite element.

Results presented in Figure 11 show excellent agreement between predictions ψ'_p and actual changes $\Delta\psi_p$, except in element 6. However, the magnitude of actual change $\Delta\psi_p$ is small compared to the magnitude of ψ'_p for this element, so accuracy of the difference is questionable.

**SHAPE DESIGN SENSITIVITY FOR IMPLANT DESIGN, $\delta b_5 = 0.05b_5$
(POINTWISE PRINCIPAL STRESS IN THE STEM AT THE STEM-CEMENT INTERFACE)**

El. No.	ψ_p^1	ψ_p^2	$\Delta\psi_p$	ψ'_p	$(\psi'_p/\Delta\psi_p \times 100)\%$
1	65.75792800	65.74896400	-0.00896400	-0.00875783	97.70
2	77.13410600	77.24745600	0.11335000	0.11608011	102.41
3	58.03037400	58.53323000	0.50285600	0.52206340	103.82
4	77.00421000	79.96762700	2.96341700	3.01203420	101.64
5	151.71708000	146.27679000	-5.44029000	-5.35753070	98.48
6	234.54156000	234.78980000	0.24824000	0.68237420	274.88
7	288.65995000	291.58509000	2.92514000	3.00576120	102.76
8	149.94087000	149.70614000	-0.23473000	-0.25492036	108.60
9	20.76092900	20.75818400	-0.00274500	-0.00277719	101.17
10	6.23888850	6.22105300	-0.01783550	-0.01811896	101.59
11	3.99426970	3.91787910	-0.07639060	-0.07985700	104.54
12	6.25765390	6.73601410	0.47836020	0.48739250	101.89
13	15.90449700	15.06538300	-0.83911400	-0.91444092	108.98
14	23.77727200	23.71259200	-0.06468000	-0.06987854	108.04

Unit: MPa

Figure 11

Shape design sensitivity results for pointwise strain energy density of cement on the bone-cement interface are given in Figure 12, for a 5% design change in design parameter b_g . The pointwise strain energy density is measured at one of the Gauss points at the bone-cement interface of each cement finite element.

Results presented in Figure 12 show excellent agreement between predictions ψ'_p and actual changes $\Delta\psi_p$, except in element 41. However, the magnitude of $\Delta\psi_p$ for this element is small compared to others.

Even though results of sensitivity analysis of a pointwise principal stress in the stem and pointwise strain energy density in the cement are given, for variations of one design parameter for each, variations of all other design parameters yield similar results. Shape design sensitivity results for pointwise principal stress in the bone at the bone-cement interface and for pointwise strain energy density in the cement at the stem-cement interface are found to be excellent.

SHAPE DESIGN SENSITIVITY FOR IMPLANT DESIGN, $\delta b_g = 0.05b_g$
(POINTWISE STRAIN ENERGY DENSITY IN THE CEMENT AT THE BONE-CEMENT INTERFACE)

El. No.	ψ_p^1	ψ_p^2	$\Delta\psi_p$	ψ'_p	$(\psi'_p/\Delta\psi_p \times 100)\%$
17	2.693386	2.864695	0.171309	0.185526	108.30
18	1.324330	1.346854	0.022525	0.025306	112.35
19	1.358676	1.373181	0.014505	0.016123	111.15
20	2.968939	2.965287	-0.003652	-0.003972	108.76
21	6.532172	6.527846	-0.004325	-0.004688	108.39
22	6.197117	6.196119	-0.000998	-0.001068	107.01
23	12.301795	12.302323	0.000528	0.000569	107.74
38	5.474089	5.847445	0.373356	0.398447	106.72
39	2.187812	2.236401	0.048590	0.053682	110.48
40	2.045186	2.077065	0.031879	0.034058	106.83
41	3.616023	3.616629	0.000606	0.000478	78.88
42	10.974028	10.976652	0.002624	0.002725	103.84
43	16.638003	16.640659	0.002656	0.002837	106.81
44	22.454411	22.455967	0.001556	0.001666	107.05

Unit: kJ/m^3

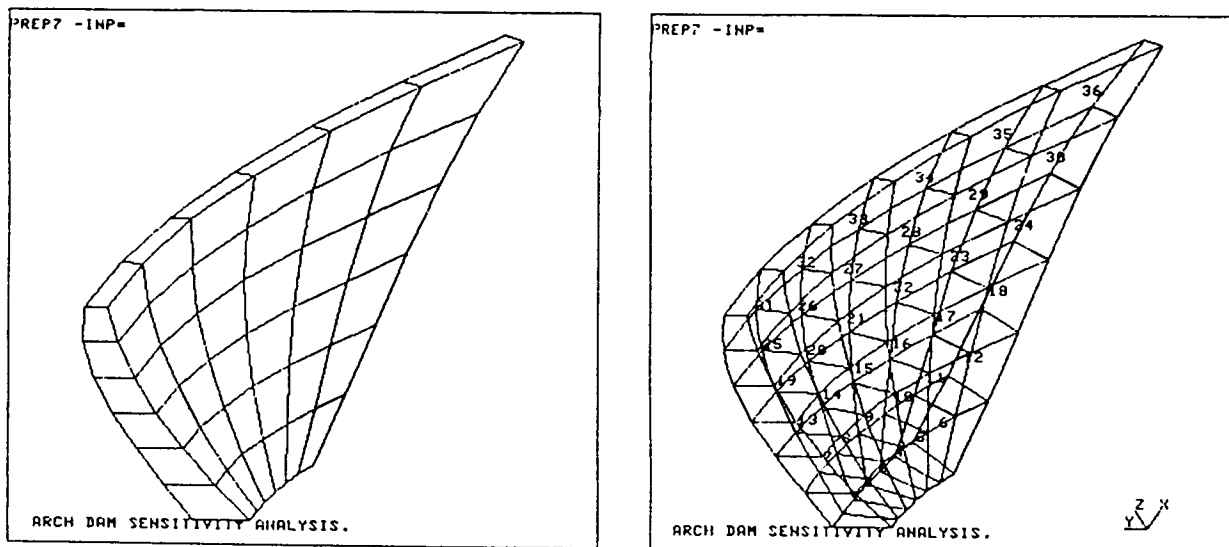
Figure 12

A doubly curved arch dam (Figure 13) that is similar to one treated by Wassermann (Ref. 15) is optimized using higher order finite-element approximation and the continuum shape design sensitivity analysis method presented here.

The dam structure and loading conditions are assumed to be symmetric with respect to the crown cross section. Thus, only half of the dam is analyzed. Also, it is assumed that the dam foundation is rigid, and the gravel concrete is homogeneous and behaves elastically. Concrete's elasticity modulus and Poisson's ratio are $E = 21.0 \text{ GPa}$ and $\nu = 0.2$, respectively. Water and concrete weight densities are 10.0 kN/m^3 and 24.0 kN/m^3 , respectively.

To parameterize two surfaces (water and free sides), Bezier surface parameterization is used with a 4×4 array of points. For a shape design parameter, the x_2 -coordinates of 32 control points are selected. The dam finite-element model contains 36 ANSYS STIF 95 elements, 315 nodal points, and 726 active degrees of freedom.

DOUBLY CURVATURED ARCH DAM



- 36 elements (ANSYS STIF95), 315 nodes, and 726 active DOF.

Figure 13

The principal stress is used as a design failure criteria. Principal stresses are measured at Gauss points on the surface of the dam (8 Gauss points for each finite element). Design sensitivity analysis results are tested for pointwise principal stresses. Excellent agreement between predictions and actual changes is obtained.

The optimal design problem for the doubly curved arch dam is to minimize the volume of the dam, subject to constraints on pointwise principal stress on the surface of dam and thickness at the top of the dam. For iterative optimization, Pshenichny's linearization method (Ref. 16) is used. History of cost function and maximum constraint violation is shown in Figure 14. After 17 design iterations, cost is reduced from an initial value of 253,566 m³ to 182,583 m³ and the maximum tensile stress is reduced from an initial value of 3.084 MPa to 1.981 MPa.

OPTIMIZATION OF DOUBLY CURVATURED ARCH DAM

- Minimize volume subject to:
 Principal stress; $-10 \text{ MPa} < \psi_i < 2 \text{ MPa}$, $i = 1, 288$
 Dam thickness; $6\text{m} < t_j$, $j = 1, 4$

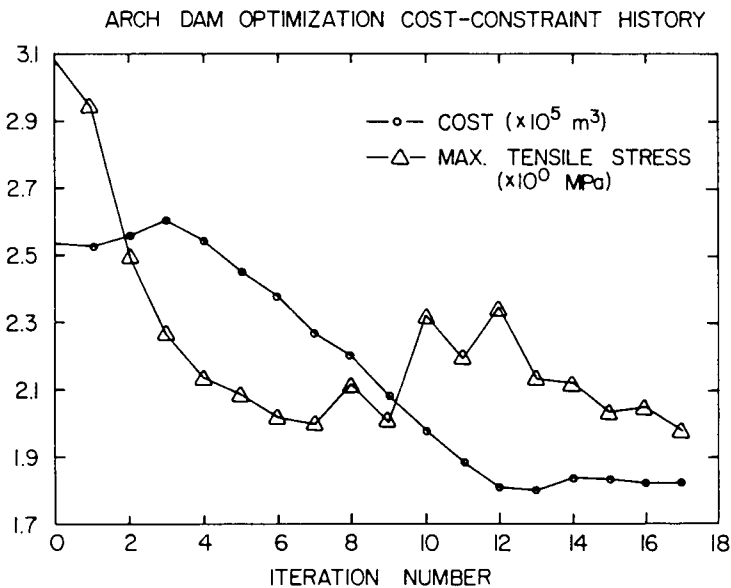


Figure 14

A profile of the final design is shown in Figure 15. The final design shown in Figure 15 is rather different from Wasserman's design (Ref. 15), mainly in the bottom portion of the dam. The final design obtained here had developed a fillet in the bottom corner, which is not observed in Wasserman's design.

In the crown cross section shown in the Figure 15, the middle portion is thinner than the top portion. From stress distribution in the final design, it is observed that the maximum tensile stress in this middle portion is well below the critical value of 2 MPa. Another interesting observation is that the compressive stress limit of -10 MPa has never been violated. In fact, at the final design, the maximum compressive stress is -5.202 MPa.

A PROFILE OF THE FINAL DESIGN

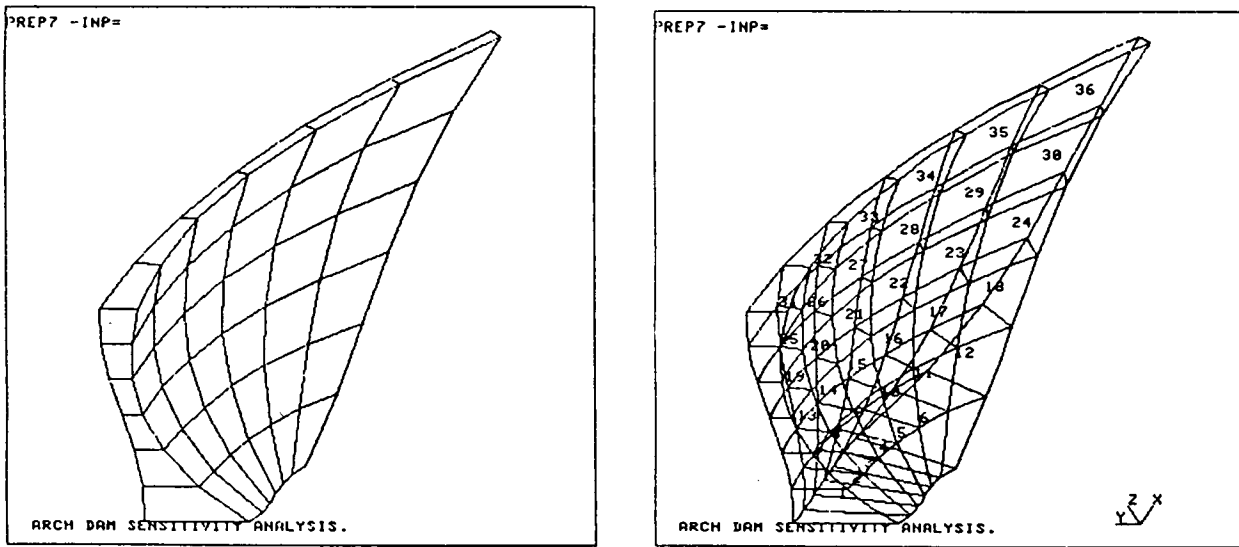


Figure 15

REFERENCES

1. Zolesio, J.P., "The Material Derivative (or Speed) Method for Shape Optimization," Optimization of Distributed Parameter Structures, (Eds., E.J. Haug and J. Cea), Sijthoff and Noordhoff, Alphen ann den Rijn, The Netherlands, 1981, pp. 1089-1151.
2. Haug, E.J., Choi, K.K., and Komkov, V., Design Sensitivity Analysis of Structural Systems, Academic Press, New York, N.Y., 1986.
3. Fung, Y.C., Foundations of Solid Mechanics, Prentice-Hall, Inc., Englewood Cliffs, N.J., 1965.
4. Choi, K.K. and Haug, E.J., "Shape Design Sensitivity Analysis of Elastic Structures," Journal of Structural Mechanics, 11(2), 1983, pp. 231-269.
5. Choi, K.K. and Seong, H.G., "A Domain Method for Shape Design Sensitivity Analysis of Built-Up Structures," Computer Methods in Applied Mechanics and Engineering, 56, 1986.
6. Mortenson, M.E., Geometric Modeling, John Wiley and Sons, New York, N.Y. 1985.
7. Choi, K.K. and Seong, H.G., "A Numerical Method for Shape Design Sensitivity Analysis and Optimization of Built-Up Structures," The Optimum Shape: Automated Structural Design, (Eds. J.A. Bennett and M.E. Botkin), Plenum Press, New York, 1986.
8. Seong, H.G. and Choi, K.K., "Boundary Layer Approach to Shape Design Sensitivity Analysis," J. of Struct. Mech., 1987.
9. Kikuchi, N., "Adaptive Grid-Design Methods for Finite Element Analysis," Comp. Meth. in Appl. Mech. and Eng., 55, 1986, pp. 129-160.
10. Thompson, J.F., Warsi, Z.U.A., and Mastin, C.W., "Boundary-Fitted Coordinate Systems for Numerical Solution of Partial Differential Equations - A Review," Journal of Computational Physics, 47, 1982, pp. 1-108.
11. Imam, M.H., Three-Dimensional Shape Optimization, General Motors Research Laboratories, Research Publications, GMR3675, 1981.
12. DeSalvo, G.J. and Swanson, J.A., ANSYS Engineering Analysis Systems, Users Manual, Swanson Analysis System, Inc., P.O. Box 65, Houston, PA, Vols. I and II, 1985.
13. Choi, K.K., Santos, J.L.T., and Frederick, M.C., "Implementation of Design Sensitivity Analysis with Existing Finite Element Codes," ASME Journal of Mechanisms, Transmissions, and Automation in Design, 85-DET-77.

14. Crowningshield, R.D. and Wilson, M.A., A Design Analysis of Bone Cements Used in Total Hip Reconstruction, A Report to Howmedica Inc., Biomechanics Laboratory, The University of Iowa, Iowa City, November, 1982.
15. Wassermann, K., "Three Dimensional Shape Optimization of Arch Dams With Prescribed Shape Functions," J. of Struct. Mech., 11(4), 1983, pp. 465-489.
16. Choi, K.K., Haug, E.J., Hou, J.W., and Sohoni, V.N., "Pshenichny's Linearization Method for Mechanical System Optimization," ASME Journal of Mechanisms, Transmissions, and Automation in Design, 106(3), 1984, pp. 415-419.